Academic Education Publishing House
Industry Science and Engineering Vol. 1 No. 7, 2024

Enhanced Fault Diagnosis of Vertical Friction Torque Using Improved VGG-CNN Network

Xiangjun Du[1,*], Ling Yu[2]
[1]*School of Mechanical Engineering, Tiangong University, Tianjin, China*
[2]*Tianjin Light Industry Vocational Technical College; Tianjin, China*
**Corresponding Author.*

Abstract: This paper presents a CNN-based fault diagnosis method utilizing Infrared Thermography (IRT) to improve the low diagnostic rates of friction torque faults in upright placements and to address bearing faults in a test bench. Employing non-destructive, non-contact infrared thermal imaging technology, the study conducts tests across six scenarios: undamaged, damaged inner ring, damaged outer ring, defective marble, insufficient lubrication, and damaged inner and outer ring bearings. This article implements a thermal image processing technique based on two-dimensional discrete wavelet transform, combining VGG Net model with CBAM attention mechanism to improve classification accuracy while reducing training time. Convolutional neural networks were then employed for fault classification and performance evaluation, demonstrating superior results compared to support vector machines. This approach effectively identifies bearing torque faults, achieving an impressive 99.80% accuracy in classifying faulty bearings, indicating its broad applicability.

Keywords: Infrared Thermography; Friction Torque; Convolutional Neural Networks; Support Vector Machines; Bearings; Fault Diagnosis

1. Introduction

Bearings, as a key component of friction torque systems, support and guide rotation under complex conditions of high speed and variable load, with failure probabilities reaching 40%. Bearing failures can result in increased noise, heightened vibration, and significant temperature rises, adversely affecting the reliability of mechanical systems [1,2]. Thus, researching fault diagnosis for bearing torque is crucial. This study demonstrates that vertical placement of friction torque bearings enhances load capacity, allowing them to better withstand forces and torques, while also reducing axial load, which benefits lifespan and performance. Additionally, vertical orientation improves lubrication and minimizes wear, as gravity helps maintain stability.

Current fault diagnosis methods include rule-based, statistical, and physical model approaches. Infrared thermal imaging (IRT) offers a non-invasive, non-contact solution for condition monitoring, delivering high accuracy and reliability [3]. Traditional mechanical fault diagnosis methods generate considerable noise and struggle to detect issues like lubricant deficiency. In contrast, IRT overcomes these limitations with its rapid, non-destructive capabilities.

Common bearing fault classification algorithms include machine learning (ML) methods such as support vector machines (SVM), k-nearest neighbors, and artificial neural networks (ANN) [4]. However, ML often requires extensive feature extraction, leading to subpar classification results. Deep convolutional networks (CNN) can automatically extract features from raw data, eliminating the need for manual intervention. Previous studies have applied CNNs to thermal imaging for bearing fault detection, yet issues like slow diagnostic speeds and low accuracy persist. Recent advancements have aimed to enhance diagnostic speed and accuracy, but challenges like overfitting remain [5].

In this article, we preprocess thermal images using two-dimensional discrete wavelet transform (2DWT) and integrate the VGG-Net model with the convolutional block attention module (CBAM) to improve performance and accuracy [6]. Our simulations demonstrate effective classification of thermal image data for various faulty bearings, showcasing strong robustness.

2. Friction Torque Test Bench and Infrared Thermal Imaging

The purpose of this study is to diagnose bearing torque faults using a friction torque test bench, simulating various faults that may occur during actual bearing operation. This approach allows for real-time monitoring and measurement to detect potential issues [7]. Utilizing ESView for precise control and adjustments, we systematically test bearings under different fault conditions to gather accurate data and results. This method enables repeatable experiments, verifying the accuracy and reliability of the findings [8]. Overall, diagnosing bearing torque faults on the friction torque test bench offers an effective and dependable means of identifying existing faults and facilitating maintenance and repair.

Experiments conducted on the bearing test bench involve various high-speed bearings to collect relevant data. The test bench employed in this research features a patented bracket designed primarily for measuring bearing friction torque, average friction torque, and starting friction torque. It consists of two main components: a mechanical execution device and a control acquisition system. The mechanical device includes a support platform, an adjustment mechanism, a replaceable clamping mechanism, and an environmental system. The control system comprises a signal acquisition device, a torque measurement system, and a data processing unit. This equipment operates within a speed range of 0 to 4500 rpm, enabling the detection of friction torque for both the shaft and bearing components under load [9]. A schematic of the experimental setup is illustrated in Figure 1.

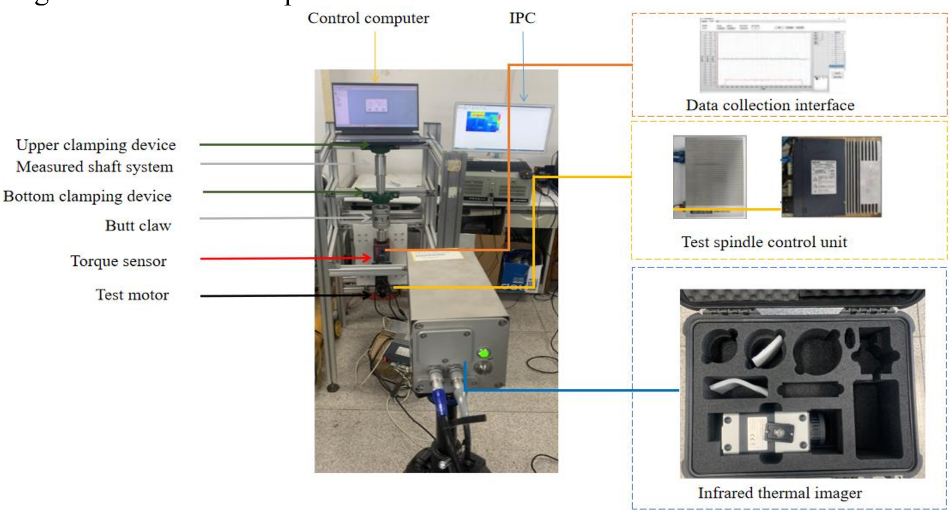

Figure 1. Experimental Device for Infrared Thermal Imaging Acquisition in Bearing Fault Diagnosis

This study utilized SKF-manufactured bearings, with detailed specifications provided in Table 1. A total of 750 images were captured at three different speeds: 300 rpm, 600 rpm, and 900 rpm, resulting in 11,250 thermal images. The dataset was divided into three parts, with 7,875 images allocated for training and 3,375 for validation. The original infrared thermal images, measuring 691×482 pixels, were cropped to 112×112 pixels to facilitate fault classification. The non-destructive bearing state served as a reference for distinguishing between different conditions [10].

The VarioCAM HD head 880 thermal imaging camera captured the infrared data at a frame rate of 30 frames per second. Sensitivity, a critical parameter, varies based on surface properties of the housing material, as well as distance, relative humidity, and temperature scale. In this experiment, the distance from the thermal imager to the target object was set at 1.5 meters to ensure high-quality image resolution [11].

The test bench was initially operated for two hours to reach a steady state before data collection commenced for eight minutes, as illustrated in Figure 3. Images were taken from the front of the test stand to capture clear representations of various fault conditions. The Figure 2 displays raw thermal images of different bearing states at 300 rpm. However, raw thermal images alone do not effectively distinguish between different fault states, underscoring the need for a self-diagnosis system utilizing intelligent algorithms.

Figure 2. (a) Inner Ring Damage (b) Inner Ring Damage (c) Outer Ring Damage (d) Lack of Lubrication

Table 1. Specifications and Characteristics of Bearings

argument	Instructions
Model number	SKF 7207CD
Contact Angle	10.583°
Pitch diameter	38.376 mm
Number of balls/rows	13
Line number	2
Sphere diameter	7.5 mm

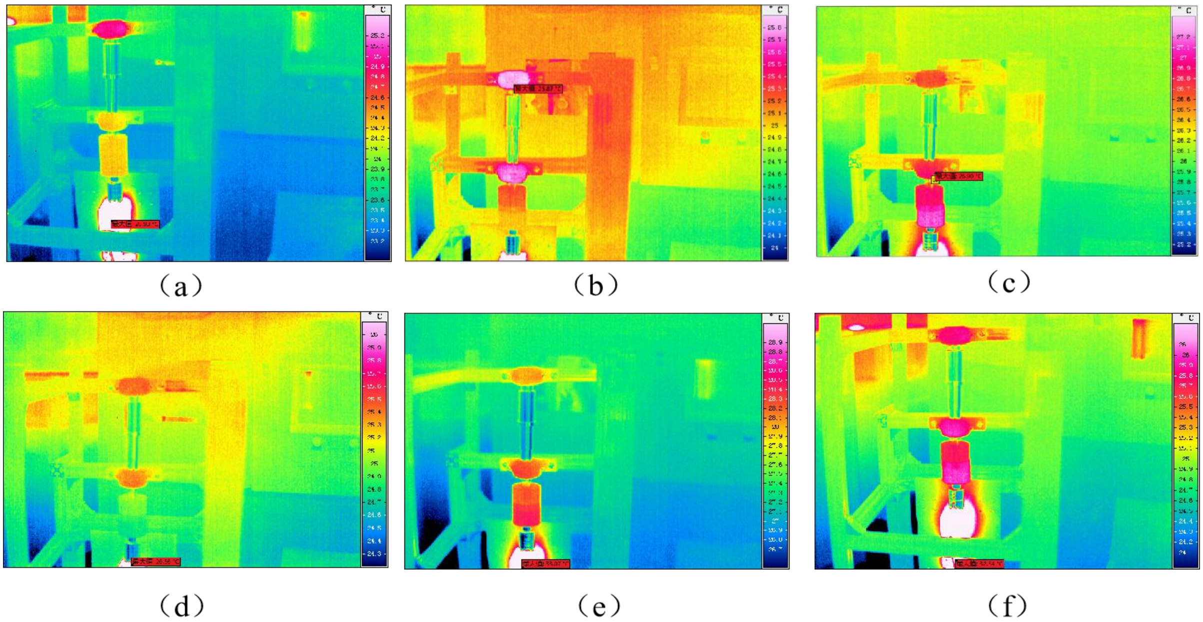

Figure 3 Raw Thermal Images of Bearings Captured at 600rpm
(a) Inner Ring Loss (b) Outer Ring Loss (c) Lack of Lubrication (d) Inner and Outer Ring Loss, Lack of Lubrication (e) Marble Defect (f) Loss

3. Diagnosis of Faults in Friction Torque Bearing

The method for diagnosing bearing faults using CNN and SVM is outlined as follows. Initially, the SVM approach involves a feature extraction and selection process specific to torque bearings. In contrast, the CNN-based method requires preprocessing and conversion of thermal images for input into the CNN. Figure 4 illustrates a schematic of the proposed diagnostic framework that integrates both CNN and SVM for bearing fault detection [12].

3.1 Preprocessing of Infrared Images for Enhanced Analysis

In this paper, infrared thermal images of friction torque bearings undergo preprocessing using discrete wavelet transform (DWT) for multi-resolution analysis in both the frequency and time domains [13]. This process yields four sub-band images of the bearings: one approximation coefficient and three detail coefficients. To isolate high and low frequency components, high-pass and low-pass filters are applied to each data line, followed by 2x downsampling. As a result, four sub-band images are generated: high-frequency detail coefficients (HH, HL), low-frequency detail coefficient (LH), and low-frequency approximation coefficient (LL) [14]. Each sub-band image exhibits unique characteristics, with high-frequency components concentrated in the detail coefficients (HH, HL, and LH) and low-frequency components found in the approximation coefficient (LL). Further decomposition of the LL band provides an even more detailed sub-band image, as illustrated in Figure 5. Here $k=0$ specifies the scale of the original image, to wit $2^k=2^0=1$. In addition, In the case of k = 1, the resulting subimage can be expressed as, the resulting subimage can be expressed as

$$\begin{gathered} t_{01}(a,b)=\left[L_x*\left[L_y*I_0\right]\right]\downarrow_2(a,b) \\ \vdots \\ t_{31}(a,b)=\left[H_x*\left[H_y*I_0\right]\right]\downarrow_2(a,b) \end{gathered} \tag{1}$$

Where (*) and (↓) represent the convolution and downsampling processes, respectively [15]. Here (Lx, Ly) and (Hx, Hy) are low-pass and high-pass filters.

t_{01} filtering and downsampling process can be expressed as.

$$Y_{low}(a,b)=\left[L_y * I_o\right]\downarrow_2(a,b)=\sum_{n=-2}^{1} I_o(a,n)L_y(a,2b-n)$$

$$t_{01}(a,b)=\left[L_x*\left[L_y * I_o\right]\downarrow_2\right]\downarrow_2(a,b)=\sum_{n=-2}^{1} Y_{low}(n,b)L_x(2a-n,b) \tag{2}$$

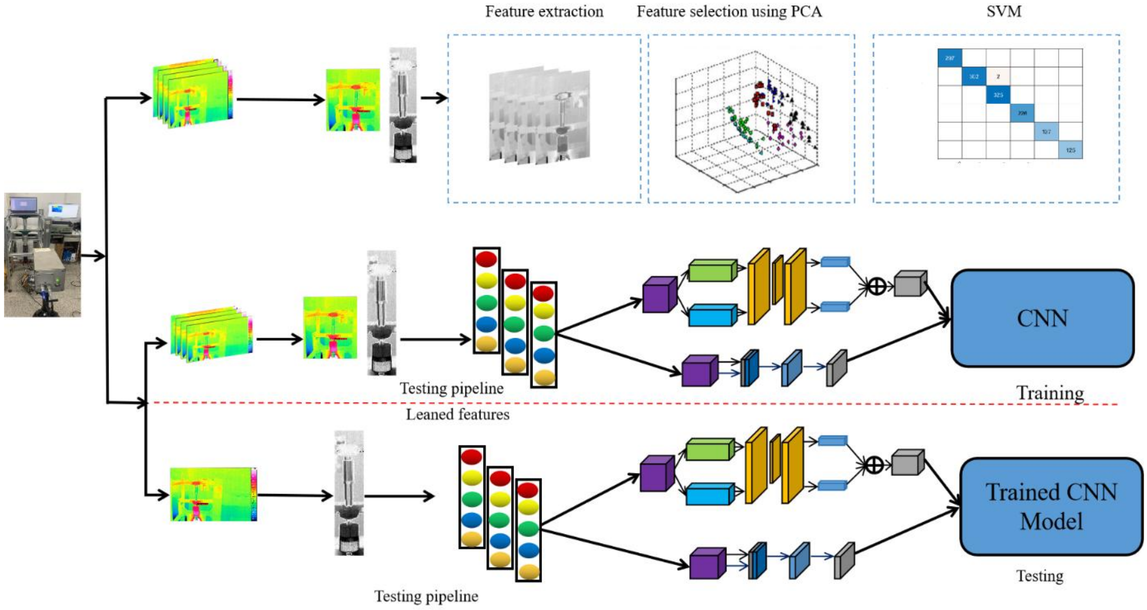

Figure 4: Flow Chart of Thermal Image Bearing Fault Diagnosis Based on CNN and SVM Proposed

To calculate t11, t21, and t31, we performed a si milar step, taking into account all decomposition levels and coefficients. The relevant feature dat a is extracted from the massive IRT data in order to classify different bearings.

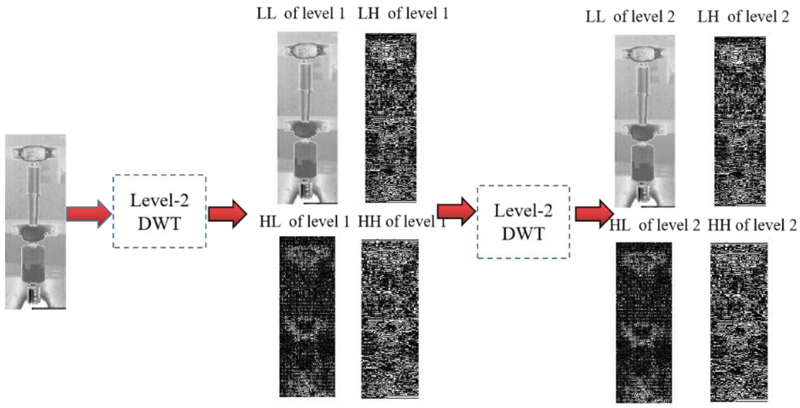

Figure 5. Two-dimensional Discrete Wavelet Transform

3.2 Friction Torque Fault Diagnosis of VGG-CBAM CNN

Convolutional neural networks (CNNs) are multi-layer feedforward architectures that utilize the backpropagation algorithm to update network parameters [15]. A typical CNN consists of convolutional layers, pooling layers, and fully connected layers. The convolutional layers perform automatic feature extraction, effectively capturing sequence features with one-dimensional convolutions. Pooling layers further refine these features by reducing data dimensions, thereby accelerating processing and mitigating overfitting.

After several rounds of convolution and pooling, the extracted features are fed into the fully connected layers for classification tasks. This structure allows CNNs to effectively differentiate between various fault conditions and orientations. In this study, we employ a CNN based on the VGG-Net architecture, primarily consisting of convolutional and pooling layers. The dataset is split into training and validation sets in a 7:3 ratio, ensuring that each category in the training set contains 750 images, while the validation set comprises the remaining images for each label [16].

3.2.1 Convolution Layer in Deep Learning Models

The convolution layer consists of an array of 2D filters that produce multiple feature maps. The pooling layer works in conjunction with the convolution layer to combine the results of local convolutions while reducing the spatial dimensions of the infrared thermal images [17]. The 2D convolution operation can be represented as:

$$B(e,f)=\sum_{m=0}^{\infty}\sum_{n=0}^{\infty}x(m,n)h(e-m,f-n) \quad (3)$$

In the convolution process, h denotes the impulse response, while m and n represent the pixel values of the input infrared thermal (IRT) image. The output pixel values after convolution are denoted as e and f. The convolution operation utilizes a sliding window to generate the output for the subsequent layer [18].

The activation function in the convolutional layer plays a crucial role in transforming the convolved IRT data by introducing nonlinear transformations. This enhances feature representation, promotes sparsity, and addresses the gradient vanishing problem, thereby improving the convolutional neural network's performance. Common activation functions include ReLU, Leaky ReLU, Sigmoid, Tanh, and Softmax. While ReLU is straightforward, it can lead to issues such as neuron death, limiting its effectiveness in extracting bearing features. Leaky ReLU helps alleviate neuron death by introducing a small slope, but selecting the appropriate slope can be challenging. Sigmoid functions are primarily suited for binary classification, making them less effective for multi-class scenarios like faulty bearings. The Tanh function also suffers from gradient vanishing, risking the loss of important fault features. In contrast, Softmax is well-suited for multi-class classification and does not face these limitations, which is why this study employs Softmax as the activation function.

3.2.2 Batch Normalization (BN) Layer for Improved Model Performance

The convolutional layer is followed by a batch normalization (BN) layer, which applies mean reduction and variance adjustment to the input data, thereby accelerating training and enhancing the model's robustness. After BN is applied to the infrared thermal imaging data, the dataset is processed using the ReLU linear activation function, as represented in equation 6. This normalization step mitigates the gradient vanishing issue often encountered in deep neural networks and enhances their ability to express non-linear relationships. Additionally, the Softmax activation function addresses gradient dispersion, improving the convergence efficiency of the bearing fault diagnosis model.

$$u=\frac{1}{N}\sum_{i=1}^{N}x_i \quad (4)$$

$$\sigma^2=\frac{1}{N}\sum_{i=1}^{N}\left(x_i-u_i\right)^2 \quad (5)$$

$$k_i=\frac{x_i-u}{\sqrt{\sigma^2+\varepsilon}} \quad (6)$$

$$y_i=\gamma k_i+\beta \quad (7)$$

Where μ denotes the average of the sample, xi represents the input properties, N indicates the total number of samples, σ is the variance, ki stands for the normalized sample value, yi is the output after scaling ki, ε is a small constant, and γ and β are the scaling parameters.

$$Z_t^l=f\left(x_t^l\right)=\max\left\{0,x_t^l\right\} \quad (8)$$

Where x_t^l indicates input and Z_t^l indicates output.

The pooling layer is typically positioned between two consecutive convolution layers and functions by reducing the size of each feature map while maintaining a constant number of feature maps [19]. Pooling operations can include maximum pooling, average pooling, and sum pooling. Maximum pooling identifies the highest value within the specified region as the output, average pooling computes the mean of the values, and sum pooling totals the values within the region.

3.2.3 Spatial Attention Module for Enhanced Feature Representation

CBAM integrates spatial and channel attention mechanisms, as illustrated in Figure 8. The network operates on two independent dimensions—channel and spatial—to derive weights for faulty bearings. When the input torque bearing feature has dimensions of H×W×C, where H, W, and C denote height, width, and the number of channels, respectively, the channel attention mechanism operates as shown in Figure 6. Initially, features undergo maximum and average pooling, resulting in a size of 1×1×C. This output is then fed into a multi-layer perceptron (MLP) with shared weights. The MLP applies a sigmoid activation function to process and aggregate the features, yielding a mapped weight MC. Subsequently, this weight is multiplied with the input features to produce new features influenced by the channel attention mechanism [20].

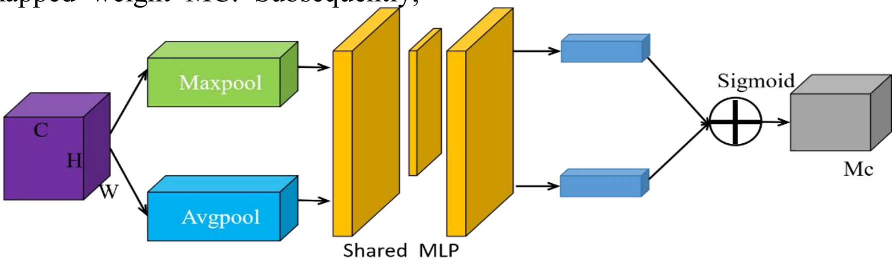

Figure 6. Enhanced Channel Attention Module for Improved Feature Representation

Spatial attention is illustrated in Figure 7. The features of the faulty bearings are combined on the channels after applying maximum pooling and average pooling, resulting in H×W×2 features. These features are then processed through a convolution kernel of size 1×7, using an S-shaped activation function to derive the weight coefficient Ms. This coefficient is multiplied by the input features to produce new features enhanced by spatial attention.

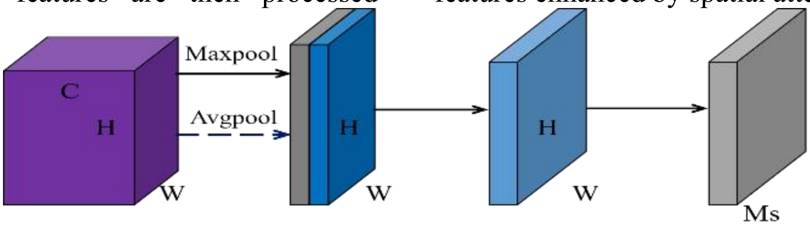

Figure 7. Spatial Attention Module for Enhanced Feature Representation

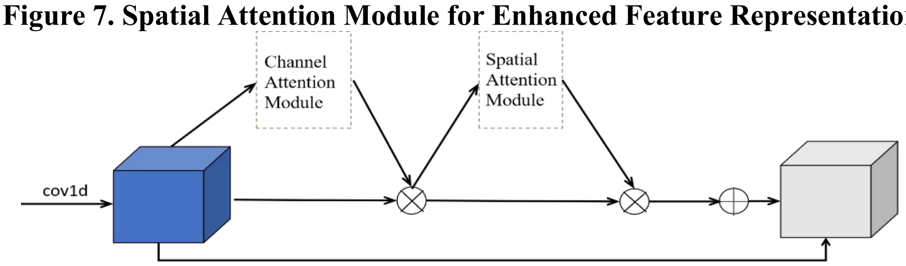

Figure 8. CBAM Attention Mechanism

By integrating the strengths of VGG-Net and the Convolutional Block Attention Module (CBAM), this model minimizes the loss of fault-bearing information during network propagation. It combines spatial attention with regularity of change, effectively focusing on the task of infrared thermal imaging (IRT) classification for bearings [21].

The algorithm model is illustrated in Figure 9. The initial size of the thermal image for friction torque bearings is 691×482 pixels, which is adjusted to an input size of 112×112 pixels. The model's output categorizes the bearings into six different states, with the output scores reflecting the probability of each bearing being in a specific state or exhibiting failure. The first layer accepts a 112×112 single-channel grayscale thermal image, which is then downsampled to 56×56 dimensions. The architecture comprises 11 convolutional layers, each with 3×3 filters, operating at five steps to produce 512 feature maps of size 7×7. The third pooling layer employs a 2×2 max pooling operation with the same stride, halving the dimensions of each feature map.

Incorporating the CBAM attention module in the middle enhances feature representation, followed by flattening the neurons to yield a total of 512 neurons. Two fully connected layers are added, culminating in an output layer with six neurons, each corresponding to a specific bearing state. For optimization, the root mean square propagation (RMSprop) algorithm is utilized to normalize the gradient.

Figure 10 presents a comparison of various improvement methods with a learning rate of 0.01 and a decay rate of 0.7. The results indicate that the CNN algorithm depicted in Figure 10 (a) experiences a low initial loss rate, but it does not converge throughout the training process, resulting in an accuracy of only 88.57%. In Figure 10 (b), incorporating the VGG-Net model leads to a reduction in loss and an improvement in accuracy to approximately 95.81%. Figure 10 (c) shows the addition of the CBAM attention module, which enhances initial training performance without significant data loss, increasing accuracy to 98.91%. Finally, Figure 10 (d) illustrates the combined approach of both methods, which enhances the verification rate, reduces iterations, and achieves 100% accuracy in bearing fault classification while maintaining the initial accuracy level [22].

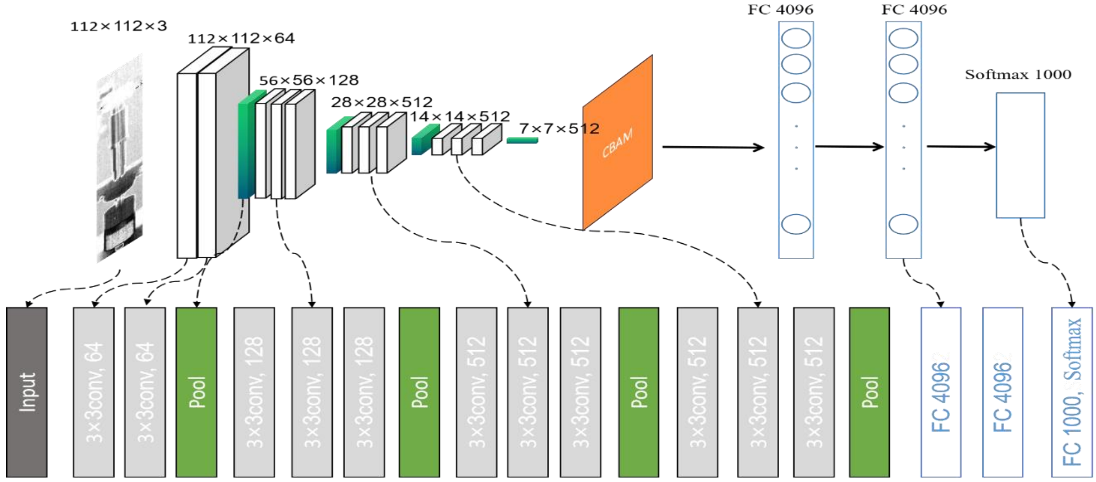

Figure 9. Proposed Network Architecture in This Study

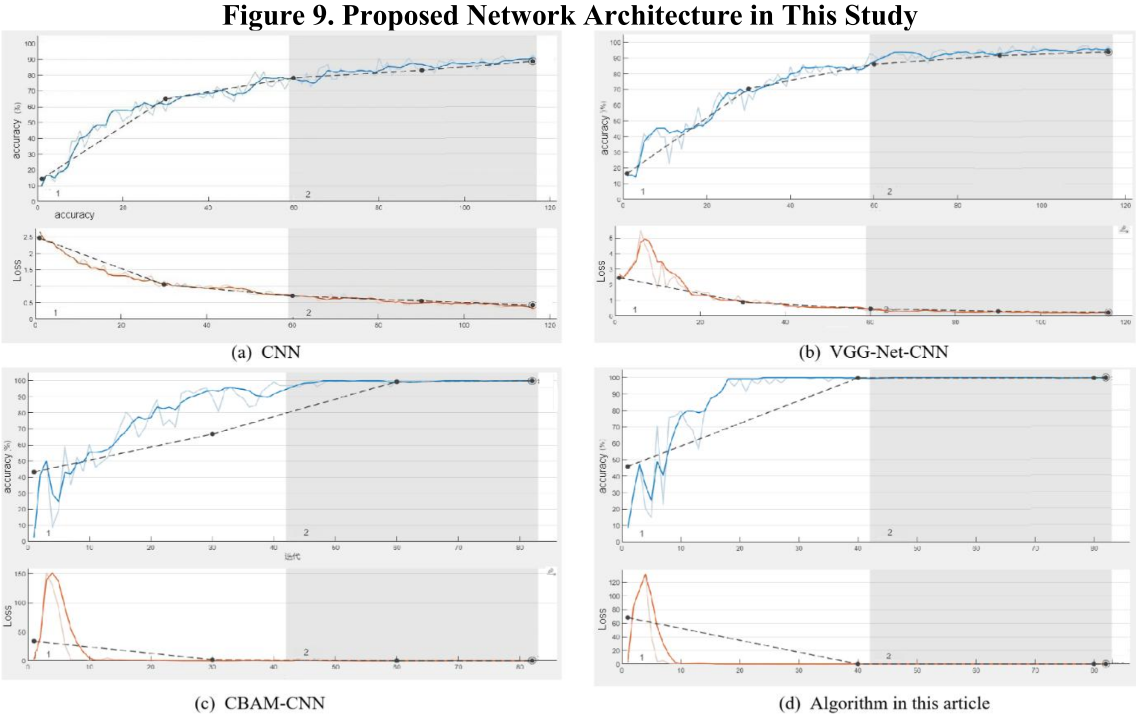

Figure 10. Comparison of Bearing Fault Diagnosis Results

3.3 Diagnosis of Friction Torque Faults Using PCA and SVM

After preprocessing the thermal images of friction torque bearings, feature extraction is performed to capture relevant information across different bearing states. Nine statistical parameters are calculated: mean (AVG), standard deviation (STD), entropy (EN), energy (E), skewness (SK), kurtosis (KU), contrast (CT), uniformity (UF), and correlation (CL). These parameters quantitatively describe the characteristics of the thermal images and serve as a crucial foundation for subsequent model training and classification. Each feature is normalized by subtracting the minimum value of the original thermal image and dividing by the range between the minimum and maximum values, resulting in a range of [0, 1].

Principal Component Analysis (PCA) is employed to identify the optimal linear transformation by calculating the covariance matrix of the normalized features, maximizing the variance of the transformed data. The features are then sorted based on their corresponding eigenvalues. By selecting a specific number of principal components, we control the variance retained from the original features, thereby determining the dimensionality of the new feature space. This dimensionality reduction helps to eliminate redundant features, preventing overfitting and enhancing model performance.

In this study, various SVM kernel functions—including linear, polynomial, Gaussian, and sigmoid—are evaluated for classification success rates. Among these, the quadratic kernel function proves most effective for handling complex multi-class data.

To classify unknown samples, we calculate the distance between features extracted from different fault cases and the lossless features. Once the distance from the known group exceeds a certain threshold, these unknown samples can be categorized accordingly. The six most significant features identified are M, KU, E, STD, EN, and KU. During this process, PCA filters out less relevant features and combines data under the same load into a 6×6 feature matrix, which serves as the input vector for further classification, facilitating SVM-based bearing fault diagnosis.

4. Experimental Results and Discussion

The performance of the proposed algorithm is compared to that of SVM. For multi-class predictions, the results are organized into a 2D confusion matrix, where each class corresponds to a "row-by-column" structure. The dimensions of the matrix reflect the count of test samples, with columns representing predicted classes and rows indicating actual classes. The evaluation of the classification process includes overall accuracy, the confusion matrix, and relevant statistical metrics.

This study assesses performance from four key perspectives: accuracy rate, precision, recall, and F1 score.

$$Accuracy = \frac{TP+TN}{TP+FP+FN+TN} \times 100\% \quad (9)$$

$$\begin{gathered} \Pr ecision = \frac{TP}{TP+FP} \times 100\%; \\ \Pr ecision_{marco} = \frac{\sum_{i=1}^{L} precision}{|L|} \end{gathered} \quad (10)$$

$$\begin{gathered} \mathrm{Re}\, call = \frac{TP}{TP \times FN} \times 100\%; \\ \mathrm{Re}\, call_{macro} = \frac{\sum_{i=1}^{L} \mathrm{Re}\, call}{|L|} \end{gathered} \quad (11)$$

$$F1score_{macro} = \frac{2 \times \Pr ecision_{macro} \times \mathrm{Re} call_{macro}}{\Pr ecision_{macro} + \mathrm{Re} call_{macro}} \quad (12)$$

4.1 Ablation Experiment

To evaluate the impact of enhanced strategies, such as the CBAM mixed domain attention mechanism and the VGG-Net network model, on fault detection performance, we conducted ablation tests. The results indicate that these improvements are effective, with Precision and score selected as the evaluation metrics. The experimental results are summarized in Table 2.

From the findings, it is evident that introducing the CBAM mixed domain attention mechanism into the backbone network (sequence number 2) improves Precision and score by 3.22% and 2.09%, respectively. This demonstrates the method's ability to effectively utilize feature information, emphasizing relevant features in the channel and reducing classification errors. In sequence number 3, the incorporation of the adaptive spatial feature fusion network VGG-Net results in a 1.8% increase in score, confirming that VGG-Net effectively mitigates the learning of irrelevant features through weight adjustments, ensuring focused feature fusion at each layer.

Sequence number 4 combines both strategies, showing that this multi-strategy approach is more effective than relying on a single enhancement. Compared to the original CNN model, Precision and score increased by 7.72% and 6.86%, respectively, indicating that the algorithm proposed in this study demonstrates strong performance in fault classification.

Table 2. Ablation Experiment

SN	CBAM	VGG-Net	Precision (%)	Score (%)
1	×	×	92.12	93.12
2	√	×	95.34	95.21
3	×	√	95.75	97.12
4	√	√	99.84	99.98

4.2 Comparison of Fault Diagnosis Outcomes: VGG-CNN vs. PCA-SVM

The bearing classification method presented in this article utilizes features extracted from the original thermal image dataset for training, categorizing six distinct bearing conditions. This study reveals that the proposed method outperforms support vector machines (SVM) in terms of accuracy and reliability in bearing fault classification. This enhanced performance may stem from the VGG-Net model's integration of prior learning concepts and regularization techniques, which help prevent overfitting.

Analysis of IRT data, simulated faults, and classifier confusion matrices in Table 3 leads to the conclusion that the proposed fault detection method reliably identifies fault types in images across various scenarios. In contrast, SVM may encounter classification errors in some instances, highlighting the advantages of this algorithm for bearing fault diagnosis. As shown in Table 4, a comparison of evaluation metrics between our supervised machine learning algorithm and PCA-SVM indicates superior performance in accuracy, precision, recall, and overall rating for our approach. These results demonstrate the high effectiveness of the proposed algorithm in diagnosing bearing faults.

Table 3. Performance Comparison of Bearing Fault Diagnosis Using PCA-SVM and VGG-CBAM-CNN

Prediction class											
PCA-SVM						VGG-CBAM-CNN					
	HB	OR	IR	BD	CD		HB	OR	IR	BD	CD
HB	741	40	52	21	41	HB	880	0	0	0	0
OR	29	755	42	45	2	OR	0	881	0	0	0
IR	52	57	768	3	1	IR	0	0	881	0	0
BD	26	22	10	821	13	BD	0	0	0	881	0
CD	38	17	44	7	824	CD	1	0	0	0	881

Table 4. Performance Metrics of PAC-SVM and VGG-CBAM-CNN

Decision (%)	PCA-SVM				VGG-CBAM-CNN			
	accuracy	Precision	Recall	F.Score	accuracy	Precision	Recall	F.Score
HB	98.21	81.23	83.11	82.56	99.83	98.23	99.51	92.97
OR	98.42	89.31	88.35	85.93	100	99.31	99.64	91.42
IR	98.64	95.21	92.42	74.74	99.83	99.21	92.42	99.48
BD	98.86	92.67	87.12	83.42	100	99.67	99.12	99.45
CD	98.57	89.42	94.23	87.95	99.31	98.42	94.23	99.51

5. Conclusion

This article introduces a method for classifying bearing fault images using CBAM and VGG-Net within a convolutional neural network (CNN) framework. Initially, thermal image data of bearings was collected and preprocessed with discrete wavelet transform. A batch normalization (BN) layer was incorporated after the convolutional layers, and the number of steps for each convolution operation was increased to enhance performance. To accommodate multi-classification scenarios and mitigate issues like gradient vanishing, we selected the Softmax activation function. Additionally, the CBAM attention mechanism was integrated to minimize information loss during network propagation.

Our research demonstrates that the CNN architecture based on the VGG-Net model significantly outperforms support vector machines (SVM) in classification accuracy within the domain of bearing fault diagnosis. Both models were trained on torque data from six different bearing conditions. The study also assessed the effectiveness of thermal imaging for diagnosing bearing faults across various fault scenarios. The proposed CNN method was validated using extensive datasets, including thermal images of bearings, achieving a classification accuracy of 99.80%. These findings underscore the advantages of this approach for diagnosing bearing torque faults.

Acknowledgments

This paper was supported by Tianjin Science and Technology Plan Project under Grant 23YDTPJC00290.

References

[1] Choudhary A, Mian T, Fatima S. Convolutional neural network based bearing fault diagnosis of rotating machine using thermal images. Measurement, 2021, 176: 109196.

[2] Choudhary A, Goyal D, Letha S S. Infrared

thermography-based fault diagnosis of induction motor bearings using machine learning. IEEE Sensors Journal, 21(2): 1727-1734, 15 Jan.15, 2021, doi: 10.1109/JSEN.2020.3015868.

[3] Li Z, Li Y, Sun Q, et al. Bearing fault diagnosis method based on convolutional neural network and knowledge graph. Entropy, 2022, 24(11): 1589.

[4] Pan R, Lin T, Li C, et al. Research on a deep learning based weld seam detection and positioning system for multi size automotive rims. Optical Precision Engineering, 2023, 31(08): 1174-1187

[5] Liu Z, Wang J, Duan L, et al. Infrared image combined with CNN based fault diagnosis for rotating machinery. 2017 International Conference on Sensing, Diagnostics, Prognostics, and Control (SDPC), Shanghai, China, 2017, 137-142, doi: 10.1109/SDPC.2017.35.

[6] Lucchi E, Roberti F, Alexandra T. Definition of an experimental procedure with the hot box method for the thermal performance evaluation of inhomogeneous walls. Energy & Buildings, 2018, 179.

[7] Jia Z, Liu Z, Vong C M, et al. A rotating machinery fault diagnosis method based on feature learning of thermal images. IEEE Access, 2019, 7: 12348-12359.

[8] Li Y, Du X, Wan F, et al. Rotating machinery fault diagnosis based on convolutional neural network and infrared thermal imaging. Chinese Journal of Aeronautics, 2020, 33(02): 427-438.

[9] Mehta A, Goyal D, Choudhary A, et al. Machine learning-based fault diagnosis of self-aligning bearings for rotating machinery using infrared thermography. Mathematical Problems in Engineering, 2021, 2021.

[10] Goyal D, Dhami S S, Pabla B S. Non-contact fault diagnosis of bearings in machine learning environment. IEEE Sensors Journal, 2020.

[11] Du Y, Tong L, Wei L, et al. Self updating control algorithm and verification of laser radar shaft friction torque detection equipment. Infrared and Laser Engineering, 2022, 51(08): 344-350

[12] Shao H, Wei L, Yi L, et al. Fault diagnosis of rotor bearing systems based on dual threshold attention generation adversarial networks and small samples under time-varying speed. Journal of Mechanical Engineering, 2023, 59(12): 215-224

[13] Wang X, Zhang H, Zhu J, et al. Fault diagnosis method for aviation high-speed bearings driven by multi head attention. Vibration and Shock, 2023,42 (04): 295-305. DOI: 10.13465/j.cnki.jvs.2023.04.035

[14] Sun S, Huang Z, Yang J. Research status and progress in infrared thermal non-destructive testing image processing. Infrared Technology, 2019,41 (12): 1133-1140

[15] Mian T, Choudhary A, Fatima S. Vibration and infrared thermography based multiple fault diagnosis of bearing using deep learning. Nondestructive Testing and Evaluation, 2023, 38(2): 275-296.

[16] Jin K, Zhang J, Wang Z, et al. Application of deep learning based on thermal images to identify the water stress in cotton under film-mulched drip irrigation. Agricultural Water Management, 2024, 299: 108901.

[17] Trejo-Chavez O, Cruz-Albarran I A, Resendiz-Ochoa E, et al. A CNN-based methodology for identifying mechanical faults in induction motors using thermography. Machines, 2023, 11(7): 752.

[18] Gana M, Achour H, Belaid K, et al. Non-invasive intelligent monitoring system for fault detection in induction motor based on lead-free-piezoelectric sensor using ANN. Measurement Science and Technology, 2022, 33(6): 065105.

[19] Goyal D, Choudhary A, Pabla B S, et al. Support vector machines based non-contact fault diagnosis system for bearings. Journal of Intelligent Manufacturing, 2019, 31(5): 1275-1289.

[20] Zhou X, Zhang H, Hao X, et al. Investigation on thermal behavior and temperature distribution of bearing inner and outer rings. Tribology International, 2019, 130: 289-298.

[21] Ullah I, Khan R U, Yang F, et al. Deep learning image-based defect detection in high voltage electrical equipment. Energies, 2020, 13(2): 392.

[22] Tieleman T, Hinton G. Divide the gradient by a running average of its recent magnitude. Neural networks for machine learning. Technical Report, 2017.